CRYSTAL GROWTH & DESIGN

Article

pubs.acs.org/crystal

Cruciform Electron Acceptors Based on Tetraindeno-Fused Spirofluorene

Debin Xia,[†,‡,⊥] Xin Guo,[§,⊥] Manfred Wagner,[‡] Martin Baumgarten,[*,‡] Dieter Schollmeyer,[∥] and Klaus Müllen[*,∥]

[†]MIIT Key Laboratory of Critical Materials Technology for New Energy Conversion and Storage, School of Chemistry and Chemical Engineering, Harbin Institute of Technology, 150001 Harbin, P. R. China

[‡]Max Planck Institute for Polymer Research, Ackermannweg 10, 55128 Mainz, Germany

[§]Dalian Institute of Chemical Physics, Chinese Academy of Sciences, 116023, Dalian, P. R. China

[∥]Johannes Gutenberg-University Mainz, Duesbergweg 10-14, 55128 Mainz, Germany

Supporting Information

ABSTRACT: Two cruciform tetraindenospirofluorene-based acceptors embedding carbonyl (**Spiro-4O**) and dicyanovinylene (**Spiro-8CN**) functionalities are synthesized in high yields. Single-crystal X-ray analysis reveals a one-dimensional $\pi-\pi$ stacking arrangement for **Spiro-4O**, while **Spiro-8CN** adopts a unique two-dimensional isotropic π-interaction. Cyclic voltammetry suggests a high electron affinity of −3.76 eV for **Spiro-8CN**. Such a packing motif and low LUMO energy for **Spiro-8CN** are important for bulk electron transport.

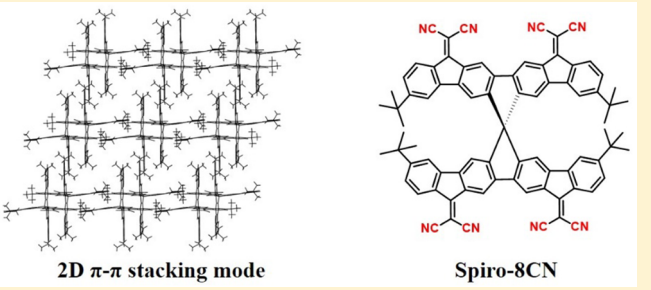

1. INTRODUCTION

The solid-state morphology of conjugated small molecules has a significant influence on the performance characteristics of electronic devices, e.g., organic field-effect transistors (OFETs)[1−3] and organic photovoltaic cells (OPVs).[4,5] Both exciton migration and charge-carrier transport are strongly modulated by the molecular packing.[6] Among the reported packing motifs, the commonly adopted arrangements with strong intermolecular overlap are edge-to-face and face-to-face modes, which hold promise to maximize electronic coupling between adjacent molecules.[7,8] Recently, several design strategies have been developed for yielding materials with a face-to-face packing motif. Holmes et al. reported that, by diminishing the CH$-\pi$ interactions, a face-to-face arrangement became accessible in crystals.[9] Chi et al. found that the attachment of fused five-membered rings to two tetracenes could change the packing structure from a herringbone arrangement to a face-to-face π-stacking mode.[10]

For organic films, the charge transport between such π-conjugated molecules is usually anisotropic, which is partially due to the effect of disordered arrangements between source and drain electrodes.[11] Materials featuring π-stacking along two directions can probably lead to isotropic charge transfer and thus also diminish the effect of random molecular orientations in thin films. Molecules which pack in the solid state along two $\pi-\pi$ stacking directions have thus attracted special interest. Cruciform structures can provide a platform for yielding materials with desired properties.[12,13] As shown in Figure 1, Samuel et al. developed a germanium spiro-center-based cruciform oligothiophene, **3D-1**, which showed a fascinating packing motif and long-range inter-chain interactions.[14] Wu et al. designed a cruciform 6,6′-dipentacenyl, **3D-2**, whose long pentacene units overlapped with the pentacene units of neighboring molecules, enabling improved macroscopic charge-carrier mobility in organic field effect transistors (OFETs).[15]

These 2D isotropic materials are p-type semiconductors, whereas materials featuring 2D isotropic electron transport have not been documented, as far as we know. This shortcoming prompted us to seek n-type 2D face-to-face π-stacking semiconductors. Herein, we introduce tetraindeno-fused spirofluorene derivatives **Spiro-4O** and **Spiro-8CN** (see Figure 1). The design principles are as follow: (i) the π-conjugated bisindenofluorene structure is planar, which facilitates good intermolecular $\pi-\pi$ stacking and favors intermolecular electronic coupling;[16−18] (ii) the spiro-carbon center gives rise to a cruciform geometry, providing possibilities for 2D intermolecular interactions;[19] (iii) the electron-withdrawing carbonyl and dicyanovinylene groups reduce the energy of the lowest unoccupied molecular orbital (LUMO), which is beneficial for electron transport;[1,20−22] and (iv) *tert*-butyl groups play a role in increasing the solubility of the rigid core and favoring single-crystal formation in comparison with long alkyl chains.[7,23]

Received: February 23, 2017
Revised: April 5, 2017
Published: April 10, 2017

DOI: 10.1021/acs.cgd.7b00272
Cryst. Growth Des. XXXX, XXX, XXX−XXX

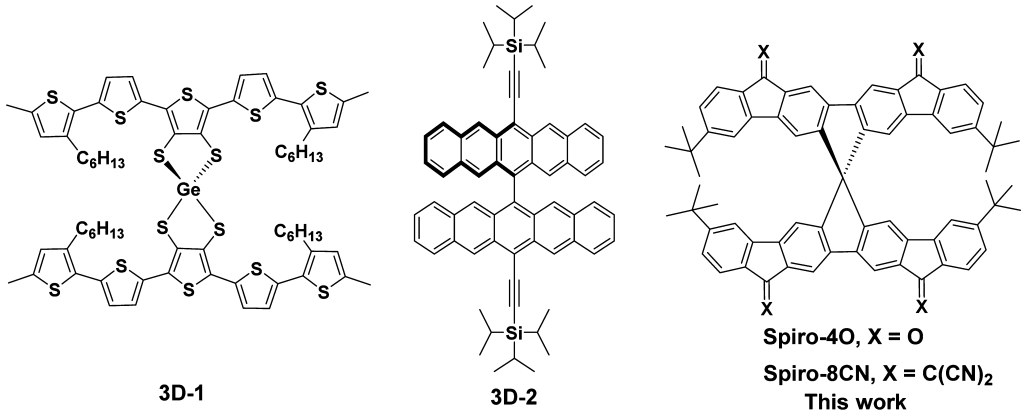

Figure 1. Chemical structures of three-dimensional p-type (**3D-1** and **3D-2**) and n-type (**Spiro-8CN**) molecules with 2D face-to-face packing.

2. EXPERIMENTAL SECTION

General Methods. ^{1}H NMR and ^{13}C NMR spectra were recorded in CD_2Cl_2 or $C_2D_2Cl_4$ on Bruker DPX 250 or 700 MHz instruments. High-resolution MALDI mass spectrometry measurements were performed on a Solarix ESI-/MALDI-ICR (9.4 T) system (Bruker Daltonics, Germany). Density functional theory (DFT) calculations were carried out with the Gaussian 09 program at the B3LYP/6-311G (d, p) level. X-ray crystallographic data were collected on a STOE IPDS 2T diffractometer with Cu Kα IμS mirror system. The structures were resolved by direct methods (SIR-2004) and refined by SHELXL-2014 (full matrix): 1005 refined parameters for **Spiro-4O** and 814 refined parameters for **Spiro-8CN**.

Synthetic Details. All reagents and solvents used for synthesis were obtained from commercial suppliers and used without further purification. Column chromatography was performed on silica gel 60 (Macherey-Nagel, Si60). 2,2′,7,7′-Tetrakis(4,4,5,5-tetramethyl-1,3,2-dioxaborolan-2-yl)-9,9′-spirobi[fluorene] was synthesized according to a reported procedure.[11] All reported yields are isolated yields.

Methyl 2-Bromo-4-(*tert*-butyl)benzoate. NaOH (15.12 g, 0.38 mol) was dissolved in 140 mL of water, followed by the dropwise addition of bromine (5.00 mL, 0.10 mol) in an ice bath. Next, a solution of 1-(2-bromo-4-(*tert*-butyl)phenyl)ethan-1-one (6.20 g, 0.024 mol) in 120 mL of dioxane was slowly added. After 12 h, the solution was acidified with concentrated hydrochloric acid and extracted with ethyl acetate (150 × 3 mL). The combined organic layers were washed with water (200 mL) and brine (200 mL) separately, and dried with Na_2SO_4. The solvent was removed under reduced pressure to give crude product 2-bromo-4-(*tert*-butyl)benzoic acid, which was purified by column chromatography with the eluent hexane/ethyl acetate (4:1). This obtained pure precursor was added into a flask with 500 mL of methanol, followed by the dropwise of concentrated sulfuric acid (2.0 mL). The mixture was heated to reflux overnight. After cooling to room temperature, the solution was concentrated, poured into water (300 mL), and extracted with DCM (200 × 3 mL). The combined organic phases were washed with saturated $NaHCO_3$ (50 × 2 mL) and dried with Na_2SO_4. After filtration, the filtrate was concentrated to give the pure methyl 2-bromo-4-(*tert*-butyl)benzoate in a 90% yield. ^{1}H NMR (250 MHz, CD_2Cl_2) δ/ppm: 7.78 (d, J = 8.2 Hz, 1H), 7.72 (d, J = 1.9 Hz, 1H), 7.44 (dd, J = 8.2, 1.9 Hz, 1H), 3.93 (s, 3H), 1.36 (s, 9H). ^{13}C NMR (62.5 MHz, CD_2Cl_2) δ/ppm: 166.66, 157.18, 131.92, 131.50, 129.44, 124.83, 121.87, 52.56, 35.28, 31.05. HRMS (TOF MS ES+): m/z calcd for $C_{12}H_{15}O_2NaBr$ 293.0153, found 293.0164.

Tetramethyl 2,2′,2″,2‴-(9,9′-Spirobi[fluorene]-2,2′,7,7′-tetrayl)tetrakis(4-(*tert*-butyl)benzoate) (1). A mixture of 2,2′,7,7′-tetrakis(4,4,5,5-tetramethyl-1,3,2-dioxaborolan-2-yl)-9,9′-spirobi-[fluorene] (2.31 g, 2.89 mmol), methyl 2-bromo-4-(*tert*-butyl)benzoate (3.6 g, 13.28 mmol), tetrakis(triphenylphosphine)palladium(0) (667 mg, 0.58 mmol), 2 M aqueous potassium carbonate solution (50 mL), and toluene (200 mL) was stirred for 2 days at 110 °C under argon atmosphere. After cooling to room temperature, the mixture was extracted with DCM (80 × 3 mL). The obtained organic layers were washed with brine, dried with Na_2SO_4, and filtered. The filtrate was concentrated under reduced pressure. After purification by column chromatography with eluent hexane/ethyl acetate (10:1), the desired compound **1** was obtained as a white solid in a yield of 74%. ^{1}H NMR (250 MHz, $C_2D_2Cl_4$) δ/ppm: 7.88 (d, J = 7.9 Hz, 4H), 7.56 (d, J = 8.0 Hz, 4H), 7.38 (dd, J = 7.8, 1.7 Hz, 4H), 7.30 (dd, J = 8.3, 1.8 Hz, 4H), 7.25 (d, J = 1.9 Hz, 4H), 6.65 (s, 4H), 3.06 (s, 12H), 1.25 (s, 36H). ^{13}C NMR (63 MHz, CD_2Cl_2) δ/ppm: 169.36, 155.13, 149.18, 141.90, 141.85, 141.03, 130.06, 128.70, 128.60, 127.98, 124.82, 124.60, 120.54, 66.28, 51.97, 35.26, 31.31. HRMS (TOF MS ES+): m/z calcd for $C_{73}H_{73}O_8$ 1077.5305, found 1077.5299.

2,2′,2″,2‴-(9,9′-Spirobi[fluorene]-2,2′,7,7′-tetrayl)tetrakis(4-(*tert*-butyl)benzoic Acid) (2). A solution of sodium hydroxide (12 g in 45 mL water) was added dropwise into a suspension of compound **1** (2.3 g, 2.14 mmol) in 300 mL of ethanol. The resulting solution was stirred for 12 h at 90 °C. After cooling to room temperature, the solution was concentrated under reduced pressure, and the residue was acidified with concentrated hydrochloric acid. The white solid product was obtained by filtration, followed by washing with water (1000 mL) and drying in the vacuum oven. Finally, pure compound **2** was obtained in a yield of 99%. ^{1}H NMR (250 MHz, CD_2Cl_2) δ/ppm: 7.84 (d, J = 7.7 Hz, 4H), 7.39 (dd, J = 12.9, 8.0 Hz, 8H), 7.29 (d, J = 8.5 Hz, 4H), 7.27 (s, 4H), 6.59 (s, 4H), 1.22 (s, 36H). ^{13}C NMR (63 MHz, CD_2Cl_2) δ/ppm: 176.32, 154.99, 148.70, 141.90, 141.84, 141.13, 129.56, 128.37, 128.23, 127.45, 124.58, 124.53, 120.63, 66.35, 35.26, 31.21. HRMS (TOF MS ES+): m/z calcd for $C_{69}H_{65}O_8$ 1021.4679, found 1021.4704.

3,3′,9,9′-Tetra-*tert*-butyl-6,6′-spirobi[cyclopenta[2,1-b:3,4-b′]difluorene]-12,12′,15,15′-tetraone (Spiro-4O). Dry DMF (0.07 mL) was added dropwise to a solution of **2** (0.60 g, 0.59 mmol) and 2 mol/L oxalyl chloride (6 mL, 12 mmol) in dry DCM (120 mL). The mixture was stirred for 10 h at room temperature. The solvent was evaporated under reduced pressure. The residue was dissolved in 30 mL of dry DCM and added to a suspension of anhydrous $AlCl_3$ (848 mg, 4.8 mmol) in dry DCM (100 mL) at 0 °C. After 12 h later, the reaction mixture was poured into ice water slowly, extracted with DCM (80 × 3 mL), dried with Na_2SO_4, and filtered. The solvent was removed, and the crude product was purified by column chromatography, using eluent ethyl acetate (20:1) to give **Spiro-4O** as a yellow solid in a yield of 82% (0.46 g). ^{1}H NMR (700 MHz, $C_2D_2Cl_4$) δ/ppm: 8.19 (s, 4H), 7.55 (d, J = 7.8 Hz, 4H), 7.27 (s, 4H), 7.24 (d, J = 7.8 Hz, 4H), 6.93 (s, 4H), 1.19 (s, 36H). ^{13}C NMR (63 MHz, $C_2D_2Cl_4$) δ/ppm: 192.54, 159.65, 153.64, 145.44, 143.83, 141.74, 135.94, 132.08, 126.64, 124.44, 117.94, 116.37, 116.12, 66.42, 35.55, 31.02. HRMS (TOF MS ES+): m/z calc. for $C_{69}H_{57}O_4$ 949.4257, found 949.4249.

2,2′,2″,2‴-(3,3′,9,9′-Tetra-*tert*-butyl-6,6′-spirobi[cyclopenta-[2,1-*b*:3,4-*b*′]difluorene]-12,12′,15,15′-tetraylidene)tetra-malononitrile (Spiro-8CN). **Spiro-4O** (0.20 g, 0.21 mmol) and malononitrile (1.39 g, 21 mmol) were dissolved in dry $CHCl_3$ (80 mL) under argon atmosphere. $TiCl_4$ (2.3 mL, 21.0 mmol) and pyridine (2.49 mL) were added dropwise. The mixture was stirred overnight at 80 °C. After the removal of solvent, the residue was subjected to column chromatography, using pure DCM as eluent to afford product **Spiro-**

DOI: 10.1021/acs.cgd.7b00272
Cryst. Growth Des. XXXX, XXX, XXX−XXX

Scheme 1. Syntheses of Spiro-4O and Spiro-8CN

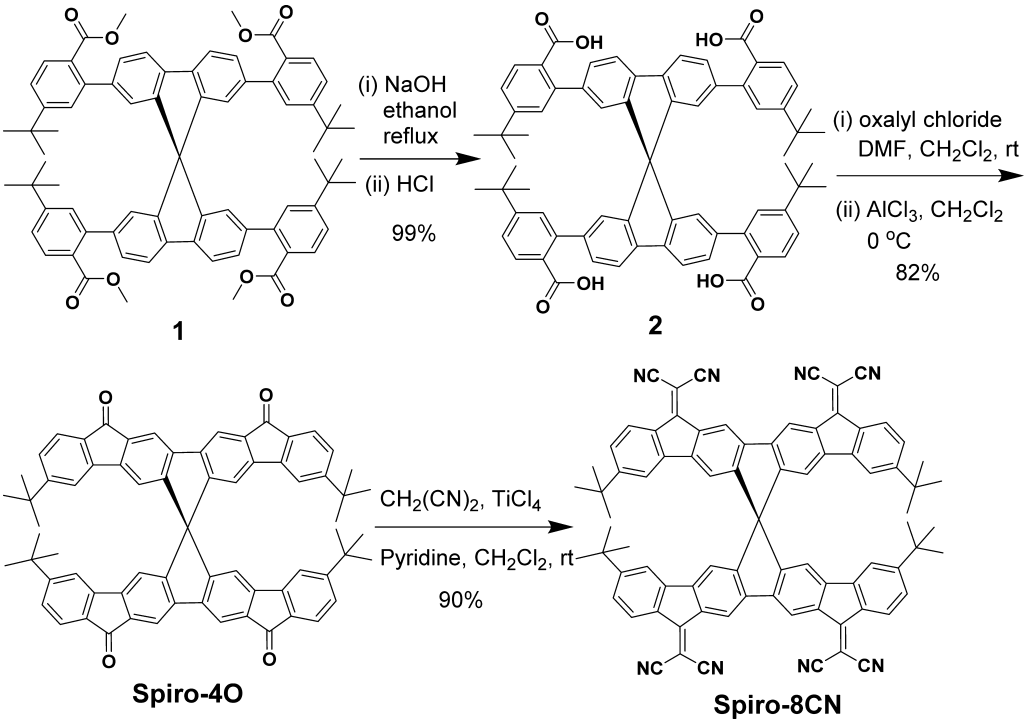

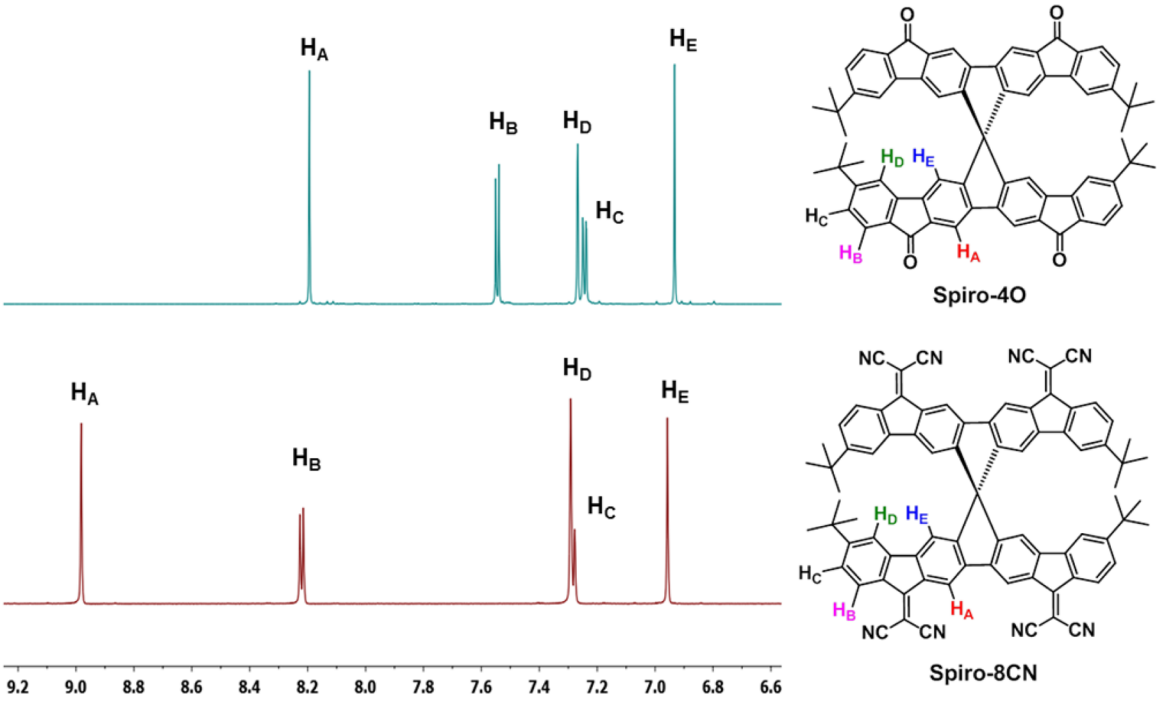

Figure 2. Aromatic region of the ^{1}H NMR spectra of **Spiro-4O** (top) and **Spiro-8CN** (bottom).

8CN as a grain solid in a yield of 90% (0.22 g). ^{1}H NMR (250 MHz, $C_2D_2Cl_4$) δ/ppm: 8.98 (s, 4H), 8.21 (d, J = 8.4 Hz, 4H), 7.30 (s, 6H), 7.27 (s, 2H), 6.97 (s, 4H), 1.20 (s, 36H). ^{13}C NMR (126 MHz, $C_2D_2Cl_4$) δ/ppm: 160.21, 159.95, 153.12, 144.02, 141.63, 141.57, 136.34, 132.35, 126.99, 126.97, 118.81, 118.09, 116.19, 113.54, 113.17, 76.30, 35.60, 30.84. HRMS (TOF MS ES+): m/z calcd for $C_{81}H_{56}N_8Na$ 1163.4526, found 1163.4541.

Cyclic Voltammetry Measurements. Electrochemistry was performed on a computer-controlled GSTAT12 in a three-electrode cell in anhydrous CH_2Cl_2, containing 0.1 M Bu_4NPF_6 as the supporting electrolyte, Ag as the reference electrode, a glassy carbon as the working electrode, Pt wire as the counter electrode. The LUMO energy levels were estimated from the onsets of the first reduction peak through the equation $E_{LUMO} = -[E_{red}^{onset} - E_{(Fc+/Fc)} + 4.8]$ eV, using ferrocene as an external standard.

3. RESULTS AND DISCUSSION

A facile synthetic route to the two rigid cruciform molecules is illustrated in Scheme 1. Compound **1** was obtained in a yield of 74% via Suzuki−Miyaura reaction between 2-bromo-4-(*tert*-

DOI: 10.1021/acs.cgd.7b00272
Cryst. Growth Des. XXXX, XXX, XXX−XXX

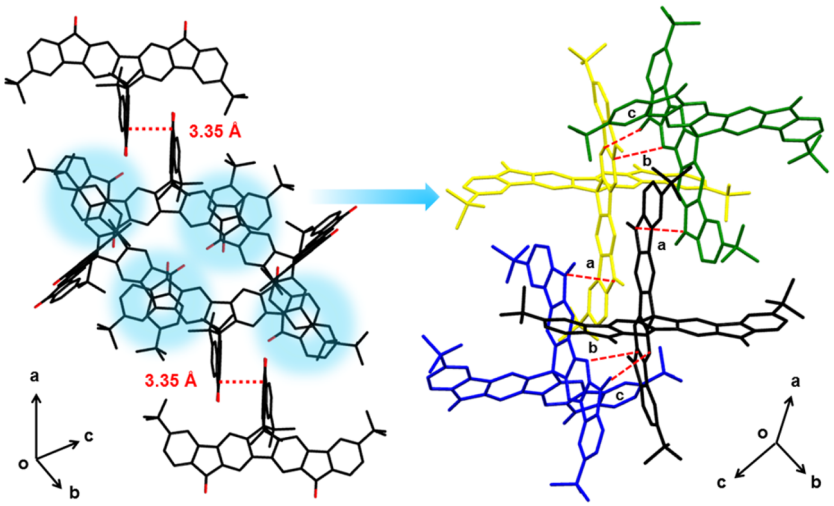

Figure 3. X-ray diffraction structure of **Spiro-4O**. (Left) Molecular stacking pattern with a $\pi-\pi$ stacking distance of 3.35 Å. (Right) Intermolecular distances: (a) 3.32 Å (C···C); (b) 3.32 Å (C···C); (c: 3.16 Å (C···O). Hydrogen atoms are omitted for clarity.

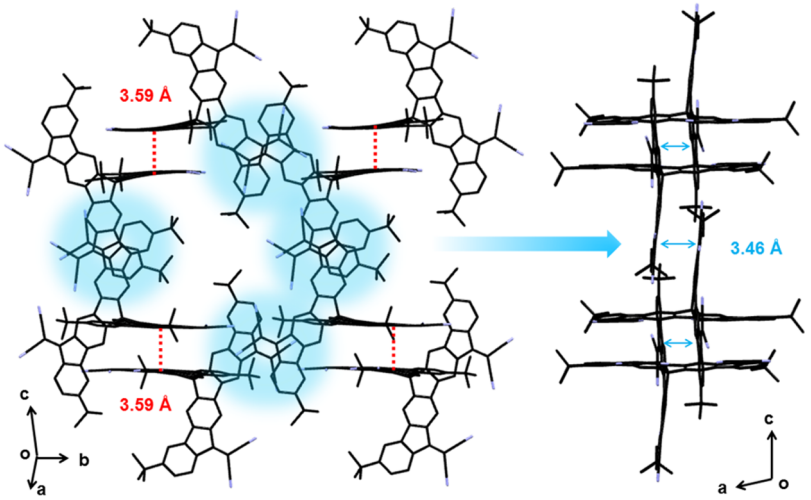

Figure 4. Molecular stacking patterns of **Spiro-8CN**. Hydrogen atoms and solvent molecules (CH_2Cl_2) are omitted for clarity.

butyl)benzoate and 2,2′,7,7′-tetrakis(4,4,5,5-tetramethyl-1,3,2-dioxaborolan-2-yl)-9,9′-spirobi[fluorene]. Hydrolysis of tetra-ester **1**, followed by acidification, gave tetraacid **2** as a colorless solid in 99% yield. Tetra-fold intramolecular Friedel−Crafts acylation was next achieved by treatment of compound **2** with oxalyl chloride and DMF. The tetraketone **Spiro-4O** was isolated as an orange solid in 82% yield. Finally, the target product **Spiro-8CN** could be obtained in 90% yield by the Knoevenagel condensation of **Spiro-4O** with the Lehnert reagent[24,25] ($TiCl_4$, malononitrile, pyridine). The overall yield of **Spiro-8CN** is 54%. Excellent thermal stabilities of **Spiro-4O** and **Spiro-8CN** were demonstrated by thermogravimetric analysis (TGA) giving high decomposition temperatures (5% weight loss) of 535 and 518 °C, respectively (Supporting Information, Figures S1 and S2).

The structures of **Spiro-4O** and **Spiro-8CN** are unambiguously confirmed by NMR spectroscopy, high-resolution MS, and single-crystal X-ray analysis. As shown in Figure 2, the assignment of all aromatic protons is obtained by a combined analysis of ^{1}H NMR, HMBC, TOCSY, and NOESY. The ^{1}H NMR spectra reveal the symmetry of both molecules and the relative strength of electron-withdrawing moieties. Due to the stronger deshielding effect, protons H_A and H_B of **Spiro-4O** and **Spiro-8CN** resonate at lower magnetic field than H_C, H_D, and H_E. Switching from carbonyl to dicyanovinylene units leads to an impressive deshielding effect for H_A and H_B of **Spiro-8CN** with chemical shifts of 8.98 and 8.22 ppm, respectively.

To investigate the solid-state packing of **Spiro-4O** and **Spiro-8CN**, single crystals of both molecules were grown by slow evaporation of the corresponding dichloromethane solutions. As expected, two π-conjugated bisfluorenone units of **Spiro-4O** or two dicyanovinylene-substituted bisindenofluorene units of **Spiro-8CN** are connected via an sp^3 carbon, which results in the formation of cruciform structures. To the best of our knowledge, **Spiro-4O** and **Spiro-8CN** are the largest cruciform oligophenylenes to date that have been characterized by X-ray diffraction. Figure 3 shows that a bisfluorenone unit of **Spiro-4O** can form slipped face-to-face π-stacking with the same unit of neighboring molecule, leading to a $\pi-\pi$ distance as short as 3.35 Å. The second bisfluorenone unit interacts with two neighboring molecules only via van der Waals forces. The right side of Figure 3 presents three types of intermolecular interactions in different directions, namely, C···C (a), C···C (b), and C···O (c), with distances of 3.32, 3.32, and 3.16 Å, respectively. For **Spiro-8CN**, a 2D $\pi-\pi$ stacking with two types of packing motifs arises due to

DOI: 10.1021/acs.cgd.7b00272
Cryst. Growth Des. XXXX, XXX, XXX−XXX

the effective parallel alignment of the aromatic rings. As shown in Figure 4, the interplanar distances for these two types of stacking are 3.59 and 3.46 Å, respectively. **Spiro-8CN** is expected to show 2D isotropic charge transport, due to its unique packing structure and the strong intermolecular interactions.

Spiro-4O and **Spiro-8CN** have good solubility in common organic solvents such as dichloromethane and THF. The UV−vis absorption spectra recorded in dichloromethane are shown in Figure 5. These two molecules provide similar absorption bands

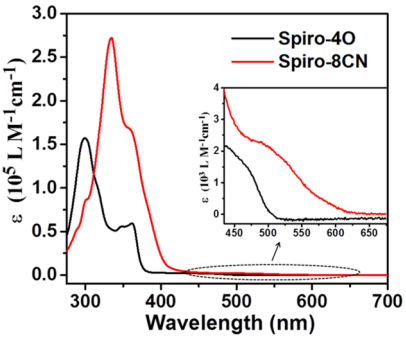

Figure 5. UV−vis absorption spectra of **Spiro-4O** (black line) and **Spiro-8CN** (red line) in CH_2Cl_2. The inset shows the UV−vis spectra in the region 440−680 nm (n−π^* transitions).

to their corresponding analogues **BE1** and **BE2** (see Supporting Information, Scheme S1),[18] which indicates that there is almost no electronic coupling between the two perpendicular bisindenofluorene moieties in **Spiro-4O** and **Spiro-8CN**. The $\pi-\pi^*$ transition of the bisindenofluorene units leads to the absorption bands in the range of 280−400 nm, reflecting a significant bathochromic shift compared to that of fluorenone.[6] This is attributed to the enhanced π-conjugation of the molecular backbone and the introduction of the electron-withdrawing groups. From **Spiro-4O** to **Spiro-8CN**, the absorption band redshifts significantly. This is mainly attributed to the decrease of the LUMO levels arising from the stronger electron-withdrawing nature of dicyanovinylene versus carbonyl substituents. The optical gap (E_g) estimated from the absorption edge of the solution spectra is 2.46 eV for **Spiro-4O** and 2.02 eV for **Spiro-8CN**, respectively.

The electrochemical properties of **Spiro-4O** and **Spiro-8CN** were investigated in CH_2Cl_2 by using cyclic voltammetry. As shown in Figure 6, reduction waves are observed, with first half-

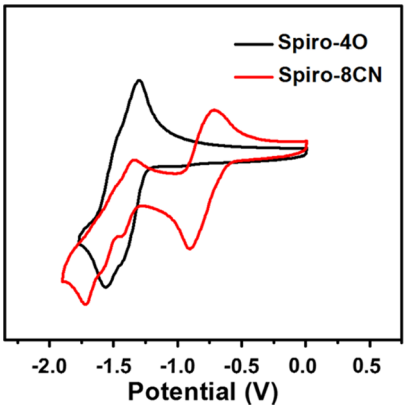

Figure 6. Cyclic voltammograms of **Spiro-4O** and **Spiro-8CN** in CH_2Cl_2.

wave potentials at −1.36 V for **Spiro-4O** and −0.81 V for **Spiro-8CN**, while no oxidation waves can be detected in the measured potential range.[4,17] The LUMO energy levels of **Spiro-4O** and **Spiro-8CN** are −3.18 and −3.76 eV, respectively, based on the first reduction potential onsets. These LUMO values are close to that of the π-conjugated bisfluorenone unit and the dicyanovinylene-substituted bisindenofluorene, respectively,[18] indicating that the spiro-carbon plays a role in interrupting the electron conjugation. The stronger electron-withdrawing character of the dicyanovinylene groups contributes to the deeper LUMO energy level of **Spiro-8CN**. The HOMO energy of **Spiro-4O** and **Spiro-8CN** are −5.51 and −5.62 eV, respectively, calculated from their optical gaps according to the equation HOMO = LUMO − E_g. Density functional theory (DFT) calculations are carried out at the B3LYP/6-311G (d, p) level. As shown in Supporting Information, Figure S3, upon going from carbonyl to dicyanovinylene groups the LUMO of **Spiro-8CN** is delocalized over the whole molecule, together with deeper energy level, which is in accordance with the CV results.

4. CONCLUSIONS

In summary, we have synthesized cruciform electron-deficient molecules **Spiro-4O** and **Spiro-8CN** in high yields. The desired 2D isotropic face-to-face π-stacking arrangement is observed for the single crystal of **Spiro-8CN**. The latter also possesses a strong electron accepting capability, with a LUMO energy as low as −3.76 eV. One expects that **Spiro-8CN** gives 2D electron transport along the π-stacking axes. The corresponding device property of OFETs is currently under investigation in our laboratory.

■ ASSOCIATED CONTENT

Supporting Information

The Supporting Information is available free of charge on the ACS Publications website at DOI: 10.1021/acs.cgd.7b00272.

Chemical structures of **BE1** and **BE2**, TGA results, DFT calculations, crystal data, and ^{1}H NMR, ^{13}C NMR, and HRMS spectra (PDF)

Accession Codes

CCDC 1408336 and 1408347 contain the supplementary crystallographic data for this paper. These data can be obtained free of charge via www.ccdc.cam.ac.uk/data_request/cif, or by emailing data_request@ccdc.cam.ac.uk, or by contacting The Cambridge Crystallographic Data Centre, 12, Union Road, Cambridge CB2 1EZ, UK; fax: +44 1223 336033.

■ AUTHOR INFORMATION

Corresponding Authors

*E-mail: martin.baumgarten@mpip-mainz.mpg.de.
*E-mail: muellen@mpip-mainz.mpg.de.

ORCID

Debin Xia: 0000-0002-2658-2577
Martin Baumgarten: 0000-0002-9564-4559
Klaus Müllen: 0000-0001-6630-8786

Author Contributions

⊥D.X. and X.G. contributed equally to this work.

Notes

The authors declare no competing financial interest.

DOI: 10.1021/acs.cgd.7b00272
Cryst. Growth Des. XXXX, XXX, XXX−XXX

■ ACKNOWLEDGMENTS

This work was financially supported by Transregio TR49, Natural Science Foundation of China (Nos. 51603055, 81601542), the China Postdoctoral Science Foundation (Grant No. 2016M601424), the Postdoctoral Foundation of Heilongjiang Province, and Key Laboratory of Functional Inorganic Material Chemistry (Heilongjiang University), Ministry of Education.

■ REFERENCES

(1) Beaujuge, P. M.; Fréchet, J. M. J. *J. Am. Chem. Soc.* **2011**, *133*, 20009−20029.
(2) Wang, C. L.; Dong, H. L.; Hu, W. P.; Liu, Y. Q.; Zhu, D. B. *Chem. Rev.* **2012**, *112*, 2208−2267.
(3) Mei, J.; Diao, Y.; Appleton, A. L.; Fang, L.; Bao, Z. *J. Am. Chem. Soc.* **2013**, *135*, 6724−6746.
(4) Mishra, A.; Bäuerle, P. *Angew. Chem., Int. Ed.* **2012**, *51*, 2020−2067.
(5) Guo, X.; Baumgarten, M.; Müllen, K. *Prog. Polym. Sci.* **2013**, *38*, 1832−1908.
(6) Anthony, J. E. *Angew. Chem., Int. Ed.* **2008**, *47*, 452−483.
(7) Liu, J.; Li, B.-W.; Tan, Y.-Z.; Giannakopoulos, A.; Sanchez-Sanchez, C.; Beljonne, D.; Ruffieux, P.; Fasel, R.; Feng, X.; Müllen, K. *J. Am. Chem. Soc.* **2015**, *137*, 6097−6103.
(8) Brédas, J. L.; Calbert, J. P.; da Silva Filho, D. A.; Cornil, J. *Proc. Natl. Acad. Sci. U. S. A.* **2002**, *99*, 5804−5809.
(9) Li, X.-C.; Sirringhaus, H.; Garnier, F.; Holmes, A. B.; Moratti, S. C.; Feeder, N.; Clegg, W.; Teat, S. J.; Friend, R. H. *J. Am. Chem. Soc.* **1998**, *120*, 2206−2207.
(10) Dai, G.; Chang, J.; Luo, J.; Dong, S.; Aratani, N.; Zheng, B.; Huang, K.-W.; Yamada, H.; Chi, C. *Angew. Chem., Int. Ed.* **2016**, *55*, 2693−2696.
(11) Ma, S.; Fu, Y.; Ni, D.; Mao, J.; Xie, Z.; Tu, G. *Chem. Commun.* **2012**, *48*, 11847−11849.
(12) Saeed, M. A.; Le, H. T. M.; Miljanić, O. Š. *Acc. Chem. Res.* **2014**, *47*, 2074−2083.
(13) Zucchero, A. J.; McGrier, P. L.; Bunz, U. H. F. *Acc. Chem. Res.* **2010**, *43*, 397−408.
(14) Wright, I. A.; Kanibolotsky, A. L.; Cameron, J.; Tuttle, T.; Skabara, P. J.; Coles, S. J.; Howells, C. T.; Thomson, S. A. J.; Gambino, S.; Samuel, I. D. W. *Angew. Chem., Int. Ed.* **2012**, *51*, 4562−4567.
(15) Zhang, X.; Jiang, X.; Luo, J.; Chi, C.; Chen, H.; Wu, J. *Chem. - Eur. J.* **2010**, *16*, 464−468.
(16) Jacques, E.; Romain, M.; Yassin, A.; Bebiche, S.; Harnois, M.; Mohammed-Brahim, T.; Rault-Berthelot, J.; Poriel, C. *J. Mater. Chem. C* **2014**, *2*, 3292−3302.
(17) Usta, H.; Facchetti, A.; Marks, T. J. *Org. Lett.* **2008**, *10*, 1385−1388.
(18) Usta, H.; Risko, C.; Wang, Z.; Huang, H.; Deliomeroglu, M. K.; Zhukhovitskiy, A.; Facchetti, A.; Marks, T. J. *J. Am. Chem. Soc.* **2009**, *131*, 5586−5608.
(19) Xia, D.; Gehrig, D.; Guo, X.; Baumgarten, M.; Laquai, F.; Mullen, K. *J. Mater. Chem. A* **2015**, *3*, 11086−11092.
(20) Shi, X.; Chang, J.; Chi, C. *Chem. Commun.* **2013**, *49*, 7135−7137.
(21) Wang, S.; Wang, M.; Zhang, X.; Yang, X.; Huang, Q.; Qiao, X.; Zhang, H.; Wu, Q.; Xiong, Y.; Gao, J.; Li, H. *Chem. Commun.* **2014**, *50*, 985−987.
(22) Yanai, N.; Mori, T.; Shinamura, S.; Osaka, I.; Takimiya, K. *Org. Lett.* **2014**, *16*, 240−3.
(23) Kohl, B.; Rominger, F.; Mastalerz, M. *Angew. Chem., Int. Ed.* **2015**, *54*, 6051−6056.
(24) Lehnert, W. *Synthesis* **1974**, *1974*, 667−669.
(25) Lehnert, W. *Tetrahedron Lett.* **1970**, *11*, 4723−4724.

DOI: 10.1021/acs.cgd.7b00272
Cryst. Growth Des. XXXX, XXX, XXX−XXX